JOURNAL OF CATALYSIS 37, 44–56 (1975)

Thermodesorption of Oxygen from Powdered Transition Metal Oxide Catalysts

B. HALPERN AND J. E. GERMAIN

Laboratoire de Catalyse organique,
Ecole Superieure de Chimie industrielle de Lyon,
69621 Villeurbanne, France

Received December 17, 1973

Flash desorption by a new technique has been applied to the study of oxygen desorption from powdered oxides of the first transition period (TiO_2, V_2O_5, Cr_2O_3, MnO_2, Fe_2O_3, Co_3O_4, NiO, CuO, ZnO).

Thermodesorption "spectra" show a small number of well-resolved peaks: one, two or three states of binding are found for oxygen, each one characterized by a calculated activation energy. Population of these states changes with preliminary treatment of the metal oxide.

The results are compared with literature data on "oxygen mobility" resulting from other experimental techniques, and with the known activity pattern of these oxides in oxidation catalysis.

INTRODUCTION

Comparison of a large number of catalyzed oxidation reactions shows that the transition metal oxides fall into a pattern of catalytic activity nearly independent of the molecule being oxidized. It is natural to ask if this pattern is related to the binding energy of active oxygen; it is also of interest to know whether this oxygen exists in discrete states or in a broad distribution of energies. The "flash desorption" technique can give information on both of these questions by displaying a spectrum of adsorbed states and permitting their energies to be measured.

The method (*1*) is to heat a surface covered with adsorbed molecules and measure a desorption flux. For molecules adsorbed in a given energy state, the increasing desorption probability and decreasing supply results in a peak in the desorption flux. If several states exist, a spectrum is obtained. From the temperature at the peak maximum, the shape of the peak, and the variation of peak position with initial coverage, one can in principle determine desorption energies and kinetics. The experimental requirements are therefore a desorption sample, a method of heating, a temperature sensor, and a desorption flux detector.

While most flash desorption experiments have been performed with metal filaments and ribbons in high vacuum, some work has been done with powdered samples. These have employed a variety of detection techniques. Cvetanovic and Amenomiya (*2*) measured concentration changes of desorbed molecules in a carrier gas with a gas chromatograph. Czanderna (*3*) studied thermodesorption from silver powder with a microbalance by relating mass change to desorption rate. Gay (*4*) obtained a desorption spectrum of oxygen on nickel oxide by measuring the rate of flow of desorbed gas through a capillary. None of these techniques requires high vacuum for its implementation. The present work

differs in this respect and so is more akin to the standard flash desorption experiment.

EXPERIMENTAL METHODS

Thermodesorption was carried out in a glass cell linked to a time-of-flight mass spectrometer, a Bayard-Alpert ionization gauge, an oxygen purification and delivery system, and an auxiliary vacuum line. These could be independently isolated by greaseless high vacuum stopcocks. The desorption cell contained a powder sample and a radiation heater.

The powder sample, or desorption source, is a cylinder of powder, 1 × 5 mm, which has been compacted and slightly sintered. A 0.1 mm Chromel–Alumel thermocouple runs along the cylinder axis, with the junction located at the midpoint. The powder is initially held around the thermocouple by a thin walled, 1 mm diameter quartz sleeve, one end of which is fire polished to a diameter of 0.1 mm, permitting passage of a thermocouple wire only. Powder placed in the sleeve is compacted by means of a thick walled capillary (bore 0.2 mm) which can slide inside the sleeve and around the thermocouple. This serves both as a piston and a means of centering the thermocouple. When the sleeve is half filled, the junction is formed by spot welding and pulled down to the powder level. The remainder of the tube can then be filled and compacted. After heating *in vacuo* to 500°C, sufficient shrinkage and sintering occurs to permit removal of the sleeve; the resulting cylinder is self-supporting though delicate, and the axial thermocouple is tightly held in good thermal contact with the powder.

Heating was effected by radiation; two types of radiation source were constructed. The first is based on the principle of the light pipe (Fig. 1). A Pyrex rod, 1 × 7 cm, is sealed at its midpoint through the glass wall of the cell. The ends of the rod are broken cleanly flat or slightly fire

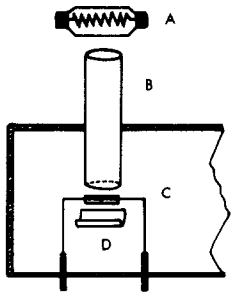

FIG. 1. Desorption cell (part). (A) 600 W bulb, (B) Pyrex rod light pipe, (C) powder cylinder and encased thermocouple, (D) gold foil mirror.

polished. The powder cylinder is positioned a few millimeters from the interior end, suspended by its thermocouple leads from an auxiliary glass frame; the leads are connected to a two-lead press seal for external contact. Radiation is supplied by a small, 600 W, iodine-vapor projection bulb, whose distance from the exterior end of the rod could be varied.

Radiant energy is conducted down the rod and onto the powder sample. A gold foil mirror, of roughly parabolic cross section, is placed behind the powder for greater efficiency and uniformity of illumination (desorption from the gold foil alone is not seen). Final temperatures of 1000°K were easily attained. The second type of radiation source was an electrically heatable platinum ribbon which could be shaped to surround, but not touch, the powder cylinder. At incandescence, radiation from the ribbon is sufficient to raise the temperature to more than 1300°K. Oxygen is desorbed from the ribbon in quantities generally small compared to the powder; this occurs rapidly before the powder heats up, so the spectra are not confused.

Oxygen gas, initially of 20 ppm purity, was contained in a 1-liter flask supplied with sidearm that had been filled with outgassed molecular sieve 13X. This serves as a condensation source. A liquid air Dewar placed around the sidearm reduces the oxygen pressure to less than a

micron. By removing the Dewar, oxygen could be admitted to the desorption cell via a stopcock and a series of liquid air cooled traps filled with quartz dust. A pressure of 200 Torr is easily obtained since little physisorption occurs on the quartz dust. The system is shown in Fig. 2.

After establishment of high vacuum, the powder was outgassed between 500 and 700°C until no further release of contaminants was detected in the spectrometer at the sensitivities employed for thermodesorption. The main impurities released were H_2O, CO_2, and a fragment at mass 30, probably NO resulting from the precipitation of the oxides from the corresponding metal nitrates. The powder is oxidized under a pressure of 200 Torr at temperatures up to 500°C for times ranging from several seconds to several minutes. After cooling to between −50 and −100°C, the oxygen was recondensed on the molecular sieve and the oxygen flask was closed off. The oxygen is thus continuously purified and repurification for each run is avoided. Thermodesorption can be commenced by establishing high vacuum, opening the desorption cell to the spectrometer, and activating the radiation source.

Because of the high internal surface area of the powder cylinder, it was found unnecessary to have initial pressures below 10^{-6} Torr since this corresponds to a recontamination rate much lower than for a flat surface. During thermodesorption only O_2 is found to desorb, and simultaneous recordings of ion gauge and spectrometer are identical; it can be concluded that the oxygen purity was sufficient for these experiments.

Commercial samples of pure grade oxides were used in most cases; sample number and surface area (BET) are given below. ZnO was precipitated from aqueous nitrate by ammonia, washed carefully, dried and calcined at 600°C for 18 hr.

TiO_2	Carlo Erba (488257)	5.5 $m^2\ g^{-1}$
V_2O_5	Carlo Erba (491121)	12.0
Cr_2O_3	Carlo Erba (440285)	6.0
MnO_2	Carlo Erba (460055)	20.0
Fe_2O_3	Carlo Erba (451826)	8.7
Co_3O_4	Prolabo (22923)	15.0
NiO	Prolabo (25885)	6.5
CuO	Prolabo (23145)	1.0
ZnO		2.6

X-Ray diffraction diagrams have been compared with published data (ASTM) and found to be consistent with the chemical formula for all oxides. TiO_2 is a mixture of rutile and anatase; iron oxide is $\alpha-Fe_2O_3$; ZnO shows an extra line (weak), presumably due to $ZnCO_3$.

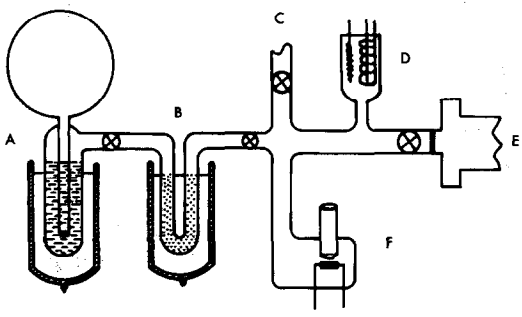

FIG. 2. Oxygen source and vacuum system. (A) Oxygen flask and molecular sieve, (B) quartz dust trap, (C) auxiliary vacuum line, (D) ion gauge, (E) time-of-flight mass spectrometer, (F) desorption cell.

RESULTS

Oxygen thermodesorption spectra were obtained for oxides of the transition metals from Ti to Zn. One, two or three binding states are found. Typical spectra and light pipe heating curves are seen in Figs. 3 and 4.

Desorption activation energies ϵ can be calculated from the general relations for first and second order desorptions:

$$e^{-\epsilon/kT_m} = \frac{\epsilon}{kT_m^2}\frac{\beta}{\nu}$$

$$e^{-\epsilon/kT_m} = \frac{1}{2\theta}\frac{\epsilon}{kT_m^2}\frac{\beta}{\nu}.$$

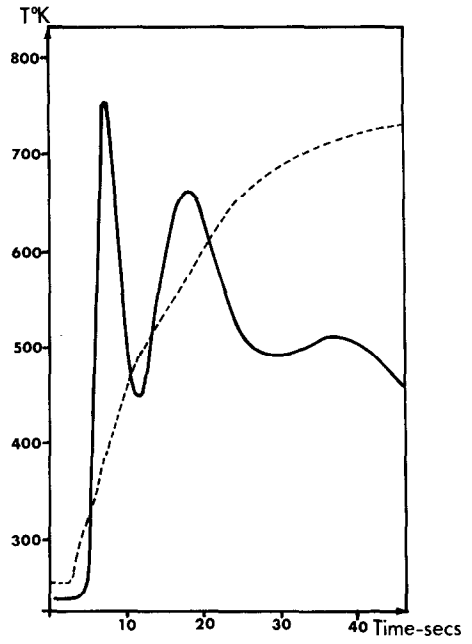

FIG. 3. Cobalt oxide (Co_3O_4) spectrum. (—) Spectrometer current; (---) heating curve.

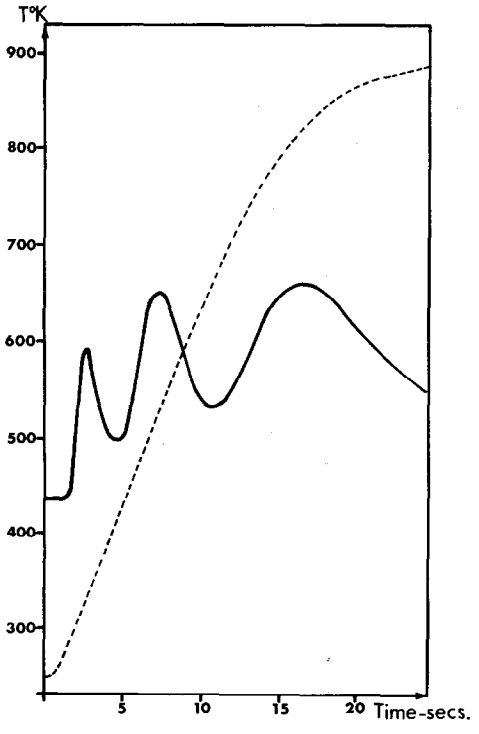

FIG. 4. Ferric oxide (Fe_2O_3) spectrum. (—) Spectrometer current; (---) heating curve.

T_m and β are the temperature and heating rate at the peak maximum, and ν is the frequency factor. For a second order process begun at full coverage ($\theta \approx 1$), the term 2θ can be expected to be of the order of unity, and neglect of this term will not incur a large error. Hence, for either a first or second order process, a good approximation to the desorption energy is (*1*):

$$\frac{\epsilon}{kT_m} = \ln \frac{\nu}{\beta} + \ln \frac{1}{T_m} \cdot \ln \frac{\nu}{\beta}.$$

ν was taken to be $kT/h = 10^{13}$ sec^{-1}; this assumes that both adsorbed molecules and activated complex are immobile. This is not unreasonable for oxygen on oxides. Independent determination of this factor is possible but requires a two order of magnitude variation of heating rate for accuracy (*5*); this cannot be done with the radiation heaters used here. Thermodesorption from powders is also potentially complicated by diffusion, readsorption (*2*), and bulk solution of oxygen. Since the main object of this work was to look for discrete states on a large group of oxides, the above simple but limited approach was adopted. The calculated energies (kcal mole^{-1}) are shown in Table 1.

A common feature of several oxides is a low energy state, state 0, adsorbed with zero or very small activation energy. All other states require elevated temperatures for adsorption. The population of state 0 is strikingly sensitive to the population of higher states. If these are filled, state 0 will be small; if empty, state 0 will be large. Beginning with a "clean" surface, a large

TABLE 1
ACTIVATION ENERGIES OF OXYGEN DESORPTION FROM OXIDES (E_d, kcal mole^{-1})

State no.	TiO_2	V_2O_5	Cr_2O_3	MnO_2	Fe_2O_3	Co_3O_4	NiO	CuO	ZnO
0				16	18.5	20	25	21	16
1	76	57.5	37	30	39	37	44	48	83
2	90		47		60	51	62		

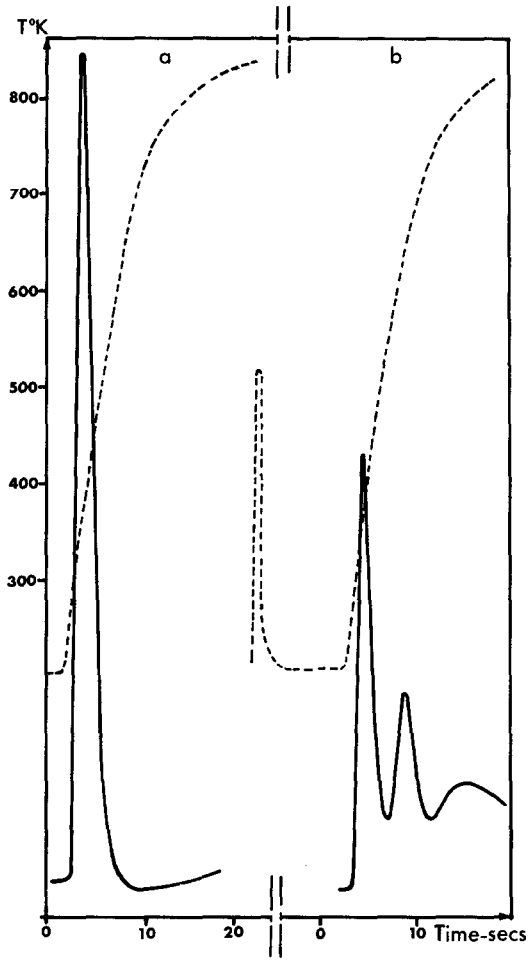

FIG. 5. Nickel oxide (NiO) state zero variation. (a) Adsorption of oxygen below room temperature; (b) oxidation at 500°K/200 Torr oxygen, several seconds.

population of state 0 can be obtained by oxygen treatment at room temperature or below; under these conditions, higher states remain empty. If oxidation is carried out at elevated temperatures, the higher states are filled and state 0 is found to have a smaller population. The effect is shown in Fig. 5 on NiO.

For MnO_2 and CuO, two states are found; the spectrum is terminated by the onset of oxide decomposition (Fig. 6). The result is interesting since it permits a qualitative comparison of the "mobilities" of chemisorbed and lattice (bulk) oxygen.

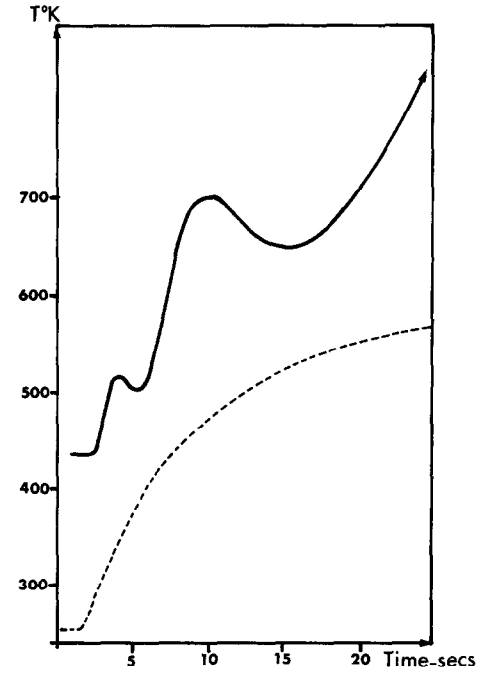

FIG. 6. Manganese oxide (MnO_2) spectrum. (—) Ion gauge current; (---) heating curve; (arrow) onset of decomposition.

Cr_2O_3 exhibits two peaks at low coverage, which are not far apart in energy. The population of the high temperature peak is much greater, however, and at high coverage the spectrum appears to have only a single peak corresponding to the higher energy (Fig. 7). The two peaks can be displayed by using a low oxidation time at a sufficiently low temperature; the higher energy state is then incompletely filled and does not overlap completely the lower state.

DISCUSSION

A. Experimental Method

Since powdered oxides *in vacuo* do not have a high thermal conductivity, one must ask if the encased thermocouple responds with sufficient rapidity to temperature

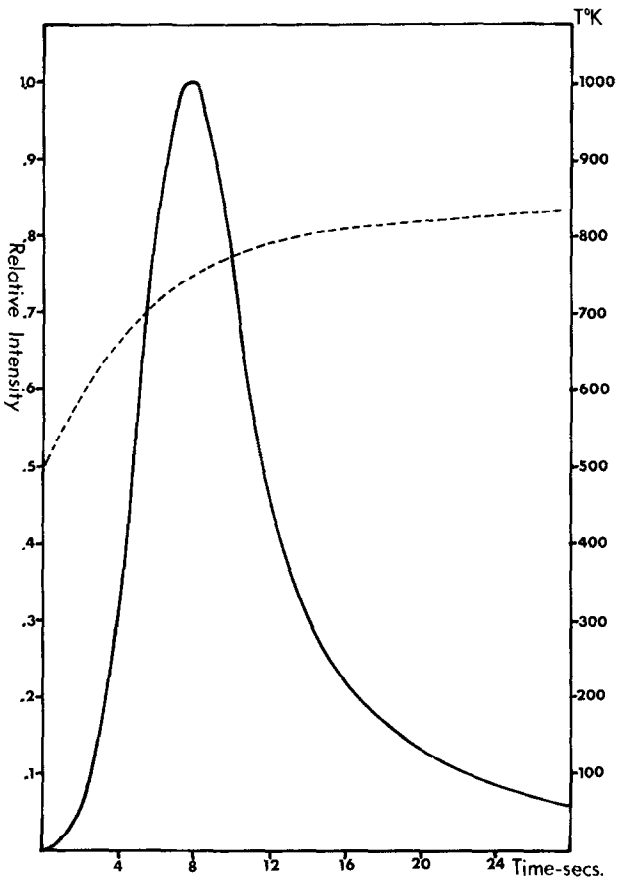

FIG. 7. Chromium oxide (Cr_2O_3) spectrum (high coverage). (—) Spectrometer current; (---) heating curve.

changes, or if significant temperature gradients exist. This question may be considered in several ways.

If the thermocouple temperature greatly lagged behind that of the outer cylinder surface, then desorption state 0 should commence and be substantially complete before the thermocouple voltage rises. This never occurs: the temperature always rises before the onset of desorption. Moreover, if the thermocouple response is slow, the stronger heating should give an apparent shift of the peak maximum to lower temperatures. This also is not seen: a higher heating rate always shifts the peak maximum to slightly higher temperatures, as would be expected (effect of β).

The thermocouple response time can be estimated as follows: energy falling on the outer surface of the sample cylinder will diffuse to the thermocouple in a time τ given roughly by:

$$\tau \sim \frac{r^2}{(K/C)},$$

where r is the cylinder radius, K the thermal conductivity, and C the heat capacity of the powder per unit volume. K will depend on the degree of sintering. If values for pressed powders (6) of $\sim 10^5$ erg cm^{-1} sec^{-1} are assumed, then heat diffusion times of less than 0.1 sec result.

An attempt to measure this time was made by using the thermocouple simultaneously as a heater and temperature sensor. Alternating current passing

through the thermocouple cannot affect the dc temperature dependent voltage. Short circuiting of this voltage by the transformer is prevented by the capacitor. Temperatures measured during current passage are accurate to ~30°C; this is verified by breaking the heating circuit and noting that the thermocouple voltage remains briefly at the same value before the onset of slow cooling. A large current, sufficient to cause a bare thermocouple to glow, is then applied suddenly. The recorded thermocouple voltage is found to rise rapidly to 100–200°C due to Joule heating; thereafter it rises slowly, at a rate determined by the heat capacity C of the powder. The duration of the rapid rise can be taken as a measure of the "damping time" of the powder. It is of the order of tenths of a second; this is adequate for peak scan times of several seconds.

The thermocouple sensitivity is sufficient to detect the melting of V_2O_5: a sudden flattening of the voltage–time curve is observed. The melting point found in this way is about 650°C, which compares well with the reported value of 670°C (*6*). Desorbing molecules, since they carry off energy, should also distort the voltage–time curve. This is a small effect for the powders studied, since the surface area per gram and adsorbed oxygen concentration are both low; nevertheless the effect is visible for Co_3O_4 (Fig. 3) as a slight kink in the heating curve for both the first two peaks.

Early experiments were carried out by heating an uncompacted powder in a gold foil dish to which a thermocouple had been spotwelded. The spectra obtained were poorly resolved and the temperatures were not meaningful since the contact between foil and powder was poor. The present construction overcomes these difficulties.

B. Diffusion and Readsorption

A molecule desorbed in the interior of the powder cylinder can be delayed by diffusion and readsorption. Since these effects can shift the peak maximum, it is of interest to estimate their importance.

In the absence of readsorption a molecule will diffuse from the center of the cylinder in a time t_d given by

$$t_d \approx \frac{r^2}{4D},$$

where D is the diffusion coefficient and r the cylinder radius. The powder cylinder can be crudely regarded as permeated by radially oriented capillaries of radius a. For Knudsen diffusion in such capillaries, $D = (2/3)ac$, where c is the molecular velocity; for the relatively low surface area powders used here, a will be taken as approximately 10^{-5} cm. The diffusion time is then $\sim 10^{-2}$ sec which cannot affect the spectrum.

Readsorption is possible during diffusion because of the large number of collisions made with powder particles. The length L corresponding to unit readsorption probability will be estimated for a bare surface. Let p be the probability of adsorption on a single collision. The number of collisions per second with the capillary wall is $\sim c/a$ and the time t_d required to diffuse the distance L is given by

$$t_d = \frac{L^2}{4D} = \frac{3L^2}{8ac}.$$

The condition for unit adsorption probability is thus

$$\frac{c}{a} \cdot \frac{3L^2}{8ac} \cdot p = 1,$$

from which L can be determined provided an assumption is made concerning p. For a diatomic molecule adsorbed via an immobile activated complex, the adsorption probability per collision is given by (*7*):

$$p = n_0 \frac{h^2}{2\pi mkT} \frac{h^2}{8\pi^2 IkT} e^{-\alpha/kT},$$

where n_0 number of sites per cm^2 ($\sim 10^{13}$)
m molecular mass ($\sim 5 \times 10^{-23}$ g)
I moment of inertia ($\sim 2 \times 10^{-38}$ gcm^{-2})
α activation energy of adsorption

Assuming a low activation energy (~ 7 kcal mole^{-1}) and a high temperature (~ 1000°K), one finds a readsorption length L of several centimeters. Since this is much longer than the cylinder radius, it is unlikely that readsorption will occur. This justifies the use of the standard thermodesorption equations.

C. *Peak Shapes*

Peak shapes characteristic of first and second order desorptions have been calculated for linear and hyperbolic heating curves by several authors (*1,5,8*). The radiation heating curve differs from these in that it is concave downwards. To show qualitatively the peak shape distortions caused by this curvature, the heating curve

$$\frac{T}{T_0} = -\frac{1}{\ln(t/\tau)}$$

will be assumed. The region of interest is $0 < t/\tau < 0.1$. By varying T_0 and τ, curves resembling radiation heat curves may be generated. It is also worth noting that a highly linear region is found for $0.1 < t/\tau < 0.3$. The function is convenient because it permits a simple integration of the differential equations for first and second order desorptions. These are:

$$\dot{\theta} = -\nu\theta e^{-\epsilon/kT} \qquad \text{1st order,}$$

$$\dot{\theta} = -\nu\theta^2 e^{-\epsilon/kT} \qquad \text{2nd order.}$$

The desorption flux is proportional to $\dot{\theta}$; the resulting equations are easily found to be

$$\dot{\theta} \propto \left(\frac{t}{t_m}\right)^n \exp\left[-\frac{n}{n+1}\left(\frac{t}{t_m}\right)^{n+1}\right] \qquad \text{1st order,}$$

$$\dot{\theta} \propto \frac{(t/t_m)^n}{\left[\frac{1}{\theta_0} + [n/(n+2)]\,(t/t_m)^{n+1}\right]^2} \qquad \text{2nd order.}$$

The parameter n is given by ϵ/kT_0; it determines the shape of the peak. The lower the value of n, the greater the distortion from the linear heat curve case. t_m is the time at which a peak maximum occurs; this was found by setting the first derivative of $\dot{\theta}$ to zero:

$$t_m^{n+1} = \frac{nt^n}{\nu} \qquad \text{1st order,}$$

$$t_m^{n+1} = \frac{1}{\theta_0}\left(\frac{n+1}{n+2}\right)\frac{nt^n}{\nu} \qquad \text{2nd order.}$$

Finally the relative coverages at the peak maximum are given in terms of θ_0 by:

$$\frac{\theta_m}{\theta_0} = e^{-n/(n+1)} \qquad \text{1st order,}$$

$$\frac{\theta_m}{\theta_0} = \frac{1}{1 + n/(n+2)} \qquad \text{2nd order.}$$

The experimental peak for Cr_2O_3 is shown in Fig. 7; it can be compared with the theoretical first and second order curves of Fig. 8 for $\theta_0 = 1$. T_0 and τ were chosen to give the experimental temperature at the peak maximum. To give the same t_m, slightly different values of n, determined by trial and error, were used for first and second order peaks, corresponding to less than 1 kcal mole^{-1} difference in energy; this does not affect the peak shape. From n and T_0, the calculated value of activation energy (45.5 kcal mole^{-1}) is in good agreement with experiment (Table 1).

Compared with peaks resulting from a linear heating curve, the first order peak is less sharply attenuated, and the second order peak is no longer Gaussian, but has developed a pronounced tail. The difference is still sufficient to distinguish the desorption order. Oxygen desorption from Cr_2O_3 thus appears to be second order,

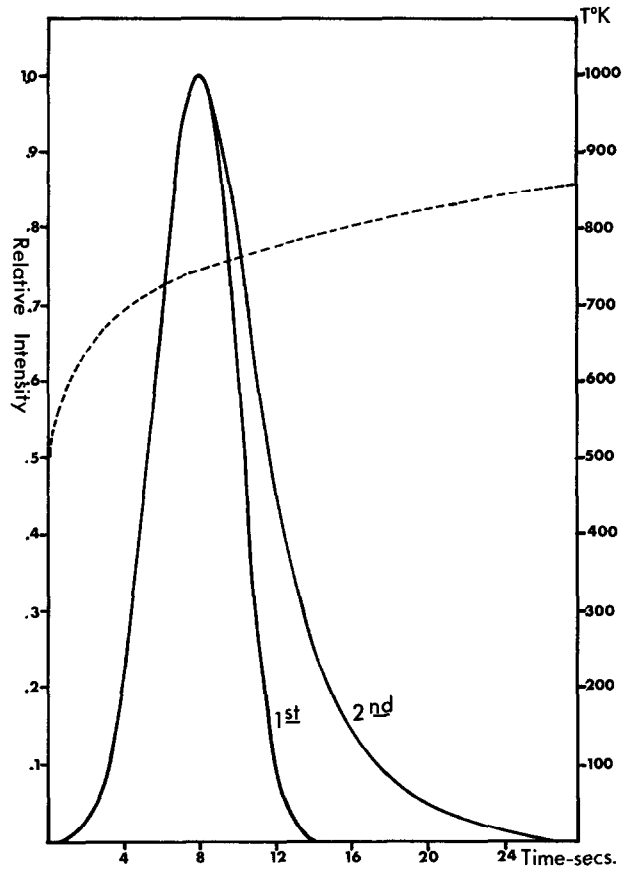

FIG. 8. First and second order desorption peaks. (—) Theoretical desorption flux ($n = 3.29$); (---) heating curve ($T_0 = 7028°K$, $\tau = 10^5$ sec).

and the peak maximum is indeed found to shift to higher temperatures with decreasing initial coverage as expected in thermodesorption (*1*).

D. Spectra and Energies

The activation energies E_d calculated from the thermodesorption spectra (Table 1) have been compared with values of desorption heats E obtained from oxygen pressure measurements on the same powders (*9*). The existence of states sufficiently separated in energy should be manifested by a series of steps in a plot of desorption heat vs coverage. Each step should correspond to a desorption peak, the activation energy E_d being equal to or slightly greater than the equilibrium adsorption (desorption) energy E. In several cases, such steps were seen (NiO, Fe_2O_3, Cr_2O_3, CuO), and the energies E_d and E were in reasonable agreement.

Steps in an E–θ plot and peaks in a desorption spectrum can also result from repulsive interactions. Wang (*10*) calculated E–θ curves for a cubic array of adsorbed molecules with nearest neighbor interaction; these curves can show an abrupt step at $\theta = 0.5$. On the oxides studied here, where only a small fraction of the surface is involved in adsorption, this would imply the existence of discrete islands of close packed sites, rather than scattered sites. Such a picture is proven false from thermodesorption spectra. If repulsive interactions existed, then the

weakly bound fraction would only give a desorption peak when the surface was at least half filled. On all spectra obtained, however, the filling of the states depended only on the oxidation conditions; high and low energy states appeared in arbitrary proportions. It can be concluded that for oxygen adsorption on oxides, repulsive interactions cannot explain the experimental facts.

Very similar spectra are obtained from samples of a given oxide prepared in various ways and give, within a 10% range of error, the same desorption energies. The reproducibility of runs on the same sample is much better (about 5%). The pattern arising from the values of E_d reported above (Table 1) therefore permit us to enter into a general discussion of the binding energy of active oxygen. Several attempts have been made in the past to characterize the "oxygen mobility" of common oxides of the transition metals (*11*). Boreskov *et al.* (*12*), (*14*), have measured the temperature dependence of the oxygen equilibrium pressure on oxides heated in a closed vessel (isochore method); the heats of desorption E calculated from a Clausius-Clapeyron plot (log P vs $1/T$) were found to increase sharply, in most cases, with the amount of oxygen removed from the sample. Initial values after a standard treatment at 500°C under an oxygen atmosphere are given in Table 2. A good correlation was found with the activation energies of oxygen isotopic exchange on the same catalysts (*13*).

On each oxide, the heat of desorption E increases monotonically, according to Boreskov *et al.*, from a low initial value (Table 2) to the high value expected for oxide decomposition. The obvious conclusion was that mobile oxygen occupied a broad and continuous distribution of states on the oxide. In contrast to this, our flash desorption results (Table 1) indicate that mobile oxygen exists on each oxide in a small number (1 to 3) of discrete states.

This discrepancy was cleared up by a careful reinvestigation of the isochore method (*9*) carried out in this laboratory: the curve of desorption heat vs amount of oxygen desorbed actually shows in many instances a number of steps corresponding to the number of peaks in the flash desorption spectrum. However, the state of lowest energy may be easily missed with some oxides due to experimental difficulties.

Correlations between activity and oxygen mobility in catalytic oxidations implies a knowledge of the oxygen states involved in the catalysis. For a given system, this state could change with temperature, partial pressures of oxygen and reagents, and the time when several states of oxygen coexist; each one could be responsible for a particular reaction of the same oxidizable molecule.

If the observed states are labeled according to Table 1, a comparison with the data of Boreskov *et al.* (Table 2) shows that the first species detected by the isochore method are oxygen in state 1 for Ti, V, Cr, Fe and Zn oxides, but oxygen in state 0 for Co, Ni and Cu oxides, as illustrated in Fig. 9. The parallelism between heat of desorption and activation energy for catalytic oxygen isotope exchange (Table 2) indicates that the same states of oxygen are the catalytic species in this reaction. The same pattern of catalytic activity:

$$TiO_2 < V_2O_5 < Cr_2O_3 < MnO_2 < Fe_2O_3 < Co_3O_4 < NiO < CuO < ZnO$$

is also observed in the oxidation of hydrogen, ammonia, methane, ethylene, and other hydrocarbons (*11*) with excess ox-

TABLE 2
HEATS OF OXYGEN DESORPTION (STANDARD STATE) FROM OXIDES (E, kcal mole^{-1})

Oxide:	TiO_2	V_2O_5	Cr_2O_3	MnO_2	Fe_2O_3	Co_3O_4	NiO	CuO	ZnO
E	59	43	26	20	34	16	19	18	54

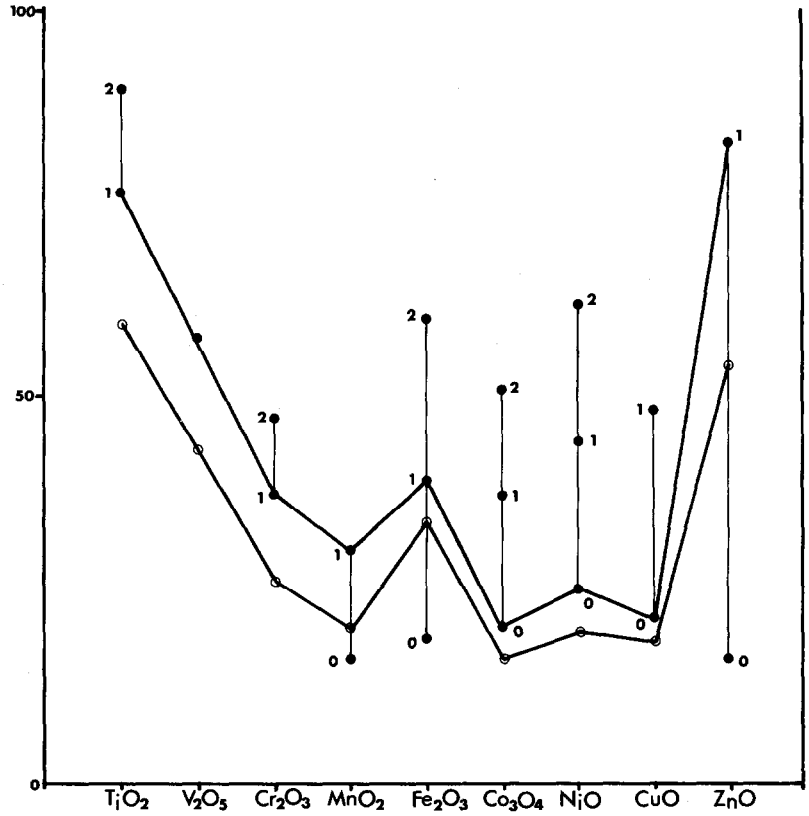

FIG. 9. Activation energies [E_d, this work (●)] and heats of desorption [E, from Ref. (*13*) (○)] of oxygen from oxides of the 4th Period (kcal mole^{-1}).

ygen and the same conclusion could be drawn in these cases.

A much higher activity of MnO_2, Fe_2O_3 and ZnO would be expected if state 0 on these oxides was operative. This seems to be the case when these oxides are degassed in vacuum at high temperature—instead of oxidized—and catalytic exchange of oxygen is run at low temperature (*14*), notably on ZnO. A very high rate of catalysis is then observed, completely unrelated with the exchange of oxide oxygen. We have shown above that high temperature oxygen treatment strongly reduces state 0, important for oxides degassed at high temperature and oxidized at low temperature.

A common feature of many oxidation reactions is a high initial rate followed by a deactivation; this could be rationalized as a progressive consumption of the most labile oxygen (state 0), the subsequent reaction being sustained on oxygen states of higher energies (states 1,2,. . .). This effect is of course magnified at very low oxygen pressures.

This shift to higher oxygen states may entail large distortions of the general activity pattern, and explains in part the difficulties met in correlating catalytic activity and oxygen mobility of oxides (*15*).

So far we have no indications about the physical nature of the different states of mobile oxygen, or different oxygen species bound to each state (O_2^-, O^-, O^{2-}). These questions have been discussed by many authors (*16,17*) and investigated using a variety of experimental techniques. Transi-

tion metal oxides are known to depart easily from stoichiometric composition (semiconductors) and lattice oxygen extraction with formation of a surface or bulk defect structure is likely to occur at moderate temperatures. A clear-cut distinction between chemisorbed and lattice oxygen is often difficult, and interconversion between both probable. It is convenient to use the term "desorbed oxygen," but this does not imply that oxygen extracted in flash desorption experiments is actually chemisorbed or surface oxygen. For example, states 0 (Table 1) could be assigned to chemisorbed oxygen, while states 1, 2, . . . could arise from the formation of different kinds of oxygen vacancies in the outer layers of the oxide lattice, or in the bulk. If chemisorption sites are identified with surface oxygen vacancies, high temperature oxygen treatment of the sample would, as observed, strongly inhibit state 0 by filling these defects with oxygen anions O^{2-}. However, existence of several surface states is not excluded, if anionic vacancies of different coordination are taken into account, or if more than one oxygen species may bind to a given type of surface site.

Infrared spectra for O_2 adsorbed on Cr_2O_3 (*18*) show a prominent band at 1000 cm^{-1} having five components in a range of 100 cm^{-1}. These are ascribed to Cr=O double bonds whose stretching frequency is modified by environmental features. They would probably lie too close in energy to be distinguished by thermodesorption; the group is most likely desorbed in a single peak at 47 kcal $mole^{-1}$. Such fine heterogeneities cannot be seen with flash desorption techniques.

On the other hand, evidence for the existence of several states of adsorbed oxygen widely separated in the energy scale is available for Cr_2O_3 (*17*), with $E = 35$ and 55 kcal $mole^{-1}$, akin to our states 1 and 2 (Table 1).

Kinetic evidence for the existence of two states of oxygen on ZnO is discussed above.

CONCLUSIONS

A small number of states are found for oxygen desorbed from powdered transition metal oxides of the 4th Period. The calculated desorption activation energies follow approximately, with a proper choice of the states, the general activity pattern of oxidation catalysis, low desorption energies implying high activities. The existence of discrete states can be used to explain discrepancies from this sequence for particular reactions, as well as the influence of preliminary treatments of catalysts. The new flash desorption technique described in this work is particularly convenient to reveal these oxygen states.

REFERENCES

1. Ehrlich, G., *in* "Advances in Catalysis" (D. D. Eley, H. Pines and P. B. Weisz, Eds.), Vol. 14, p. 256. Academic Press, New York, 1963.
2. Cvetanovic, R. J., and Amenomiya, Y., *in* "Advances in Catalysis" (D. D. Eley, H. Pines and P. B. Weisz, Eds.), Vol. 17, p. 103. Academic Press, New York, 1967.
3. Czanderna, A. W., "Vacuum Microbalance Techniques," Vol. 6, p. 129. Plenum, New York, 1967.
4. Gay, I. D., *J. Catal.* **17**, 245 (1970).
5. Redhead, P. A., *Vacuum* **12**, 203 (1963).
6. Samsonov, G. V., "The Oxide Handbook." Plenum, New York, 1973.
7. Laidler K., *in* "Catalysis" (P. Emmett, Ed.), Vol. 1, p. 198. Reinhold, 1954.
8. Smith, A. W., and Aranoff, S., *J. Phys. Chem.* **62**, 684 (1958).
9. Joly, J. P., and Germain, J. E., unpublished data.
10. Wang, J. S., *Proc. Roy. Soc. Ser. A* **161**, 127 (1937).
11. Germain, J. E., *Intra-Science Chem. Rep.* **6**, 101 (1972).
12. Sazonov, V. A., Popovskii, V. V., and Boreskov, G. K., *Kinet. Katal.* **9**, 307, 312 (1968).
13. Boreskov, G. K., Popovskii, V. V., and Sazonov, V. A., *Proc. Int. Congr. Catal. 4th,* (Moscow) *1968* **1**, 439 (1971). (Pap. 33).
14. Boreskov, G. K., *in* "Advances in Catalysis" (D. D. Eley, H. Pines and P. B. Weisz, Eds.), Vol. 16, 285. Academic Press, New York, 1964.

15. Germain, J. E., *J. Chim. Phys.* **70,** 1048 (1973).
16. Winter, E. R. S., *in* "Advances in Catalysis," (D. D. Eley, W. G. Frankenburg, V. I. Komarewsky and P. B. Weisz, Eds.), Vol. 10, p. 196. Academic Press, New York, 1958.
17. Stone, F. S., *in* "Advances in Catalysis" (D. D. Eley, P. W. Selwood and P. B., Weisz, Eds.), Vol. 13, p. 1. Academic Press, New York, 1962.
18. Zecchina, A., Coluccia, S., Cerruti, L., and Borello, E., *J. Phys. Chem.* **75,** 2783 (1972).